

The Crystal Structure and Crystal Chemistry of Mineral-like $\text{Cd}_5(\text{VO}_4)_2(\text{OH})_4$, a Novel Isomorph of Arsenoclasite and Gatehouseite

Ljiljana Karanović, Tamara Đorđević



Дигитални репозиторијум Рударско-геолошког факултета Универзитета у Београду

[ДР РГФ]

The Crystal Structure and Crystal Chemistry of Mineral-like $\text{Cd}_5(\text{VO}_4)_2(\text{OH})_4$, a Novel Isomorph of Arsenoclasite and Gatehouseite | Ljiljana Karanović, Tamara Đorđević | Minerals | 2022 | |

10.3390/min12121601

<http://dr.rgf.bg.ac.rs/s/repo/item/0007590>

Дигитални репозиторијум Рударско-геолошког факултета Универзитета у Београду омогућава приступ издањима Факултета и радовима запослених доступним у слободном приступу. - Претрага репозиторијума доступна је на www.dr.rgf.bg.ac.rs

The Digital repository of The University of Belgrade Faculty of Mining and Geology archives faculty publications available in open access, as well as the employees' publications. - The Repository is available at: www.dr.rgf.bg.ac.rs

Article

The Crystal Structure and Crystal Chemistry of Mineral-like $\text{Cd}_5(\text{VO}_4)_2(\text{OH})_4$, a Novel Isomorph of Arsenoclasite and Gatehouseite

Ljiljana Karanović^{1,*}  and Tamara Đorđević^{2,*} ¹ Faculty of Mining and Geology, University of Belgrade, Dušina 7, 11000 Belgrade, Serbia² Institut für Mineralogie und Kristallographie, Universität Wien, Josef-Holaubek-Platz 2, 1090 Wien, Austria* Correspondence: ljiljana.karanovic@rgf.bg.ac.rs (L.K.); tamara.djordjevic@univie.ac.at (T.Đ.);
Tel.: +381-11-6894014 (L.K.); +43-1-4277 53239 (T.Đ.)

Abstract: The pentacadmium bis(vanadate(V)) tetrahydroxide $\text{Cd}_5(\text{VO}_4)_2(\text{OH})_4$ was synthesized under hydrothermal conditions, and its crystal structure was determined with single-crystal X-ray diffraction. The investigated compound is the second known compound next to $\text{Cd}(\text{VO}_3)_2 \cdot 4\text{H}_2\text{O}$ synthesized in the $\text{CdO}-\text{V}_2\text{O}_5-\text{H}_2\text{O}$ system and crystallizes isotypically to the minerals gatehouseite, $\text{Mn}_5(\text{PO}_4)_2(\text{OH})_4$, and its As analog arsenoclasite, $\text{Mn}_5(\text{AsO}_4)_2(\text{OH})_4$. Its symmetry is orthorhombic, with a space group of $P2_12_12_1$ and unit cell parameters of $a = 19.011(4)$, $b = 6.0133(12)$, $c = 9.5411(19)$ Å, $V = 1090.7(4)$ Å³, and $Z = 4$. The structure consists of double ribbons of $M(\text{O},\text{OH})_6$ -octahedra ($M = \text{Cd}2, \text{Cd}3, \text{Cd}4$) extending along [010] interconnected by edge- and corner-shared $M(\text{O},\text{OH})_6$ -octahedra ($M = \text{Cd}1, \text{Cd}5$) and discrete, slightly distorted VO_4 tetrahedra, which form double chains of coupled polyhedra $[\text{V}1\text{O}_4-\text{Cd}5\text{O}_4(\text{OH})_2-\text{Cd}1\text{O}_5(\text{OH})-\text{V}2\text{O}_4]_n$ running along the same direction. The interesting feature is the existence of V–Cd distances (3.0934(7) and 3.1081(7) Å for V1–Cd5 and V2–Cd1, respectively), which are shorter than the sum of the van der Waals radii of 3.71 Å. The V1–V2 distances of 4.1214(9) Å are also shorter than the sum of the van der Waals radii of 4.26 Å. The O–H···O hydrogen bonds additionally link the two subunits, ribbons, and chains into a three-dimensional structure. Raman spectra confirmed the presence of the hydrogen bonds and mutually isolated VO_4 groups.

Keywords: vanadium; cadmium; hydrothermal synthesis; crystal structure; crystal chemistry

Citation: Karanović, L.; Đorđević, T. The Crystal Structure and Crystal Chemistry of Mineral-like $\text{Cd}_5(\text{VO}_4)_2(\text{OH})_4$, a Novel Isomorph of Arsenoclasite and Gatehouseite. *Minerals* **2022**, *12*, 1601. <https://doi.org/10.3390/min12121601>

Academic Editor: Emanuela Schingaro

Received: 22 November 2022

Accepted: 9 December 2022

Published: 12 December 2022

Publisher's Note: MDPI stays neutral with regard to jurisdictional claims in published maps and institutional affiliations.



Copyright: © 2022 by the authors. Licensee MDPI, Basel, Switzerland. This article is an open access article distributed under the terms and conditions of the Creative Commons Attribution (CC BY) license (<https://creativecommons.org/licenses/by/4.0/>).

1. Introduction

The natural and synthetic metal vanadates phosphates and arsenates often form tetrahedral–octahedral framework structures [1,2] with potentially interesting properties, e.g., ion conductivity, ion exchange, magnetic properties, and catalytic activities [3]. In the last two decades, metal vanadates have attracted considerable attention because of their widespread technological significance in an extensive range of applications [4,5] and references therein. The $3d$ orbital of vanadium in the energy spectrum is usually located below the analogous d orbitals of other transition metals, i.e., Zr, Ti, Nb, or Tl, and therefore the bottom conduction band is lowered to a more positive position [6]. Consequently, vanadium oxides are important candidates for visible light photocatalysis. For instance, Zn-vanadates, such as $\text{Zn}_3(\text{VO}_4)_2$ [7,8] and $\text{Zn}_3\text{V}_2\text{O}_7(\text{OH})_2(\text{H}_2\text{O})_2$ [8], as well as Cd-vanadates, such as CdV_2O_6 and $\text{Cd}_2\text{V}_2\text{O}_7$ [5], have been extensively synthesized and studied for their photocatalytic performances. However, the majority of these compounds were synthesized by applying high-temperature solid-state reactions [9,10] and references therein. In the scope of our previous research, we have proved that the hydrothermal method is effective for the synthesis of new vanadium compounds [11–15]. All these vanadates(V) were characterized structurally and, in part, by spectroscopic techniques. The title compound was obtained hydrothermally, and it represents the second known synthetic compound next

to $\text{Cd}(\text{VO}_3)_2 \cdot 4\text{H}_2\text{O}$ [16] in the $\text{CdO-V}_2\text{O}_5\text{-H}_2\text{O}$ system. Its crystal structure was refined and compared to those of other analogous $M_5(\text{XO}_4)_2(\text{OH})_4$ compounds where M are divalent Cd, Co, Cu, Mn, or Ni cations, and X are pentavalent As, P, or V cations.

2. Materials and Methods

2.1. Synthesis

In the course of the experiments aimed at the preparation of Cd-Co vanadates, a starting mixture of $\text{Cd}(\text{OH})_2$ (Alfa Products 89,297, >99%), Co powder (Merck 112,211, $\geq 99\%$), and V_2O_5 (Fluka Chemika 94,710, $\geq 98\%$) with the approximate volume ratio of 1:1:1 (the weight ratio was not recorded) was employed.

The mixture was transferred into a Teflon vessel and filled to approximately one-third of the vessel's volume with distilled water (initial pH was 6). The vessel was then enclosed in a stainless steel autoclave and heated under autogenous pressure from 293.15 to 473.15 K (4 h), held at that temperature (192 h), and slowly cooled (175 h) to room temperature. After the experiment, the final pH of the solution was 6. The reaction products were filtered, washed thoroughly with distilled water, and dried in air at room temperature. $\text{Cd}_5(\text{VO}_4)_2(\text{OH})_4$ formed yellow-brownish, transparent, prismatic crystals (yield ca. 20%) together with very small (<0.1 mm), light orange, needle-like crystals of CdV_3O_7 (yield ca. 10%), V_2O_5 (yield ca. 10%), and Cd-vanadate with apatite type-structure (yield ca. 5%). Single crystals of Cd apatite were too small for single-crystal X-ray analysis but were characterized using Raman spectroscopy.

2.2. Raman Spectrometry

To obtain further information on the vanadate groups and hydrogen bonds, single crystal Raman spectra were acquired. Raman spectra of $\text{Cd}_5(\text{VO}_4)_2(\text{OH})_4$ were measured with a Horiba LabRam-HR system equipped with Olympus BX41 optical microscope in the range between 100 and 4000 cm^{-1} . The 632.8 nm excitation line of a He-Ne laser was focused with a 50 \times objective (N.A. = 0.90) on the randomly oriented single crystal. The nominal exposure time was between 60–70 s (confocal mode, Olympus 1800 lines/mm, 1.5 μm lateral resolutions, and approximately 3 μm depth resolution). The density of the laser power was well below the threshold (25% filter was used) for possible sample changes due to intense laser-light absorption and resulting temperature increase.

2.3. X-ray Diffractometry and Crystal Structure Solution

The crystal quality of several single crystals was checked with a Nonius Kappa CCD single-crystal four-circle diffractometer (Mo tube, graphite monochromator, CCD detector frame size: 621 \times 576 pixels, binned mode) equipped with a 300 μm diameter capillary-optics collimator. The crystal, which exhibited sharp reflection spots, was chosen for data collection. A complete sphere of reciprocal space (φ and ω scans) was measured at room temperature. The intensity data were processed with the Nonius program suite DENZO-SMN [17] and corrected for Lorentz, polarization, and background effects and, by the multiscan method [18,19], for absorption.

The crystal structure was solved with the SHELXT structure solution program and refined on F^2 by full-matrix least-squares using SHELXL-2018/3 [20,21] and WinGX [22]. Starting from the atomic coordinates and the labeling used for gatehouseite [23], Cd and V atoms were located. Other atomic positions were found using difference Fourier syntheses. Anisotropic displacement parameters were refined for all nonhydrogen atoms. H atoms from hydroxyl groups were located in a difference Fourier map and then refined with the distance restraint $\text{O-H} = 0.82(1)$ Å and constrained to ride on the corresponding O atom with $U_{iso}(\text{H}) = 1.5U_{eq}(\text{O})$. Crystal data, information on the data collection, and results of the final structure refinement are compiled in Table 1. Fractional atomic coordinates and equivalent isotropic displacement parameters for $\text{Cd}_5(\text{VO}_4)_2(\text{OH})_4$ are given in Table 2, the selected bond lengths in Table 3, bond valences in Table 4, and hydrogen bonds in Table 5. All drawings of structure were produced with ATOMS [24].

Table 1. Crystal data, data collection, and refinement details for $\text{Cd}_5(\text{VO}_4)_2(\text{OH})_4$.

| Chemical Formula | $\text{Cd}_5\text{H}_4\text{O}_{12}\text{V}_2$ |
|--|--|
| Temperature | 293 |
| Formula weight, M_r (g/mol) | 859.91 |
| Space group (No.), Z | Orthorhombic, $P2_12_12_1$, 4 |
| a (Å) | 19.011 (4) |
| b (Å) | 6.0133 (12) |
| c (Å) | 9.5411 (19) |
| V (Å ³) | 1090.7 (4) |
| $F(000)$, ρ_{calc} (g/cm ³) | 1544, 5.237 |
| Absorption coefficient, μ (mm ⁻¹) | 11.26 |
| $T_{\text{min}}/T_{\text{max}}$ | 0.399/0.552 |
| Crystal size (mm ³) | 0.10 × 0.08 × 0.06 |
| Crystal detector distance (mm) | 40 |
| Frame rotation width (°) | 1 |
| Total no. of frames | 1032 |
| Collection time per frame (s) | 150 |
| h, k, l ranges | ±26, ±8, ±13 |
| Absorption correction | Multi-scan |
| Reflections collected/unique | 12,585/3180 |
| Observed reflections [$I > 2\sigma(I)$] | 3079 |
| R_{int} | 0.026 |
| $2\theta_{\text{max}}$ (°) | 30 |
| Extinction coefficient, k [a] | 0.00064 (8) |
| Refined parameters | 185 |
| R indices [$I > 4\sigma(I)$] | $R_1 = 0.015$ $wR_2 = 0.036$ |
| R indices (all data) | $R_1 = 0.016$ $wR_2 = 0.036$ |
| Goodness of fit, S | 1.08 |
| $(\Delta/\sigma)_{\text{max}}$ | 0.001 |
| $(\Delta\rho)_{\text{max}}, (\Delta\rho)_{\text{min}}$ (e ⁻ Å ⁻³) | 0.74; -1.00 |
| a, b [b] | 0.0159, 1.4781 |

[a] $F_c^* = kF_c [1 + 0.001'F_c^2\lambda^3/\sin(2\theta)]^{-1/4}$; [b] $w = 1/[\sigma^2(F_o^2) + (aP)^2 + bP]$.

Table 2. Fractional atomic coordinates and equivalent isotropic displacement parameters for $\text{Cd}_5(\text{VO}_4)_2(\text{OH})_4$.

| Atom | x | y | z | $U_{\text{iso}}^*/U_{\text{eq}}$ (Å ²) |
|------|-------------|--------------|------------|--|
| Cd1 | 0.43166(2) | 0.27295(6) | 0.75333(4) | 0.01236(8) |
| Cd2 | 0.47036(2) | -0.05464(6) | 0.39132(4) | 0.01098(7) |
| Cd3 | 0.28220(2) | -0.06980(6) | 0.35388(3) | 0.01123(8) |
| Cd4 | 0.37741(3) | 0.44179(6) | 0.37772(4) | 0.01280(8) |
| Cd5 | 0.31528(3) | 0.57571(6) | 0.99733(4) | 0.01303(8) |
| V1 | 0.37572(4) | 0.11180(12) | 1.06892(6) | 0.00862(11) |
| V2 | 0.37360(4) | -0.19731(12) | 0.68339(8) | 0.00850(15) |
| O1 | 0.45222(18) | 0.2654(6) | 0.5217(4) | 0.0137(7) |
| H1 | 0.4911(15) | 0.321(10) | 0.523(7) | 0.021 * |
| O2 | 0.29638(18) | 0.6100(6) | 1.2347(4) | 0.0129(7) |
| H2 | 0.2569(15) | 0.554(10) | 1.240(7) | 0.019 * |
| O3 | 0.45626(17) | 0.6368(6) | 0.2526(4) | 0.0141(7) |
| H3 | 0.427(3) | 0.683(10) | 0.196(5) | 0.021 * |
| O4 | 0.21431(18) | 0.7472(6) | 0.9713(3) | 0.0124(7) |
| H4 | 0.203(3) | 0.789(10) | 1.050(3) | 0.019 * |
| O5 | 0.35026(17) | 0.5523(6) | 0.7643(4) | 0.0132(6) |
| O6 | 0.37237(19) | -0.2267(6) | 0.5019(4) | 0.0126(6) |
| O7 | 0.3196(2) | 0.0164(6) | 0.7275(4) | 0.0170(8) |

Table 2. Cont.

| Atom | <i>x</i> | <i>y</i> | <i>z</i> | U_{iso}^*/U_{eq} (Å ²) |
|------|-------------|------------|-----------|--------------------------------------|
| O8 | 0.45553(18) | −0.1139(7) | 0.7297(4) | 0.0166(8) |
| O9 | 0.37949(18) | 0.1117(5) | 0.2501(4) | 0.0117(6) |
| O10 | 0.29428(19) | 0.2058(6) | 1.0171(4) | 0.0151(7) |
| O11 | 0.43564(19) | 0.2935(6) | 0.9938(4) | 0.0158(7) |
| O12 | 0.39246(19) | 0.8495(6) | 1.0155(4) | 0.0156(7) |

Table 3. Bond distances and average lengths (Å) for Cd₅(VO₄)₂(OH)₄.

| Distance <Mean> | Bond Lengths (Å) | Distance <Mean> | Bond Lengths (Å) |
|------------------------|------------------|------------------------|------------------|
| Cd1—O1 | 2.245(4) | Cd2—O3 ⁱⁱ | 2.271(4) |
| Cd1—O8 ⁱ | 2.256(4) | Cd2—O11 ⁱⁱⁱ | 2.287(3) |
| Cd1—O5 | 2.287(3) | Cd2—O3 ^{iv} | 2.295(4) |
| Cd1—O11 | 2.299(4) | Cd2—O1 | 2.317(4) |
| Cd1—O8 | 2.381(4) | Cd2—O6 | 2.378(4) |
| Cd1—O7 | 2.642(4) | Cd2—O9 | 2.408(3) |
| <Cd1—O> | 2.352 | <Cd2—O> | 2.326 |
| Cd3—O4 ^v | 2.241(4) | Cd4—O1 | 2.244(4) |
| Cd3—O2 ^{vi} | 2.252(3) | Cd4—O3 | 2.246(4) |
| Cd3—O10 ^{vii} | 2.282(3) | Cd4—O4 ^v | 2.265(4) |
| Cd3—O7 ^{vii} | 2.302(4) | Cd4—O2 ^{viii} | 2.293(4) |
| Cd3—O9 | 2.365(3) | Cd4—O6 ^{ix} | 2.321(3) |
| Cd3—O6 | 2.413(4) | Cd4—O9 | 2.329(3) |
| <Cd3—O> | 2.309 | <Cd4—O> | 2.283 |
| Cd5—O4 | 2.193(3) | | |
| Cd5—O12 | 2.212(3) | | |
| Cd5—O10 | 2.268(4) | | |
| Cd5—O2 | 2.302(4) | | |
| Cd5—O5 | 2.325(3) | | |
| Cd5—O11 | 2.849(4) | | |
| <Cd5—O> | 2.358 | | |
| V1—O12 ^{iv} | 1.688(3) | V2—O8 | 1.695(4) |
| V1—O10 | 1.721(4) | V2—O7 | 1.698(3) |
| V1—O9 ^x | 1.731(4) | V2—O6 | 1.741(4) |
| V1—O11 | 1.733(4) | V2—O5 ^{iv} | 1.749(3) |
| <V1—O> | 1.718 | <V2—O> | 1.721 |

Symmetry codes: (i) $-x + 1, y + 1/2, -z + 3/2$; (ii) $-x + 1, y - 1/2, -z + 1/2$; (iii) $-x + 1, y - 1/2, -z + 3/2$; (iv) $x, y - 1, z$; (v) $-x + 1/2, -y + 1, z - 1/2$; (vi) $x, y - 1, z - 1$; (vii) $-x + 1/2, -y, z + 1/2$; (viii) $x, y, z + 1$; (ix) $x, y + 1, z$; (x) $x, y, z + 1$.

Table 4. Bond valences and bond valence sum Σv_{ij} (v.u.) for Cd₅(VO₄)₂(OH)₄*.

| Site | Cd1 | Cd2 | Cd3 | Cd4 | Cd5 | V1 | V2 | Σv_{ij} ** |
|-----------------|------------|------------|-------|-------|-------|-------|-------|--------------------|
| O1 | 0.398 | 0.328 | | 0.399 | | | | 1.125 |
| O2 | | | 0.389 | 0.349 | 0.341 | | | 1.079 |
| O3 | | 0.3710.348 | | 0.397 | | | | 1.116 |
| O4 | | | 0.402 | 0.377 | 0.458 | | | 1.237 |
| O5 | 0.355 | | | | 0.321 | | 1.157 | 1.834 |
| O6 | | 0.278 | 0.253 | 0.324 | | | 1.182 | 2.037 |
| O7 | 0.136 | | 0.341 | | | | 1.328 | 1.805 |
| O8 | 0.3860.275 | | | | | | 1.339 | 2.001 |
| O9 | | 0.256 | 0.288 | 0.317 | | 1.215 | | 2.076 |
| O10 | | | 0.360 | | 0.374 | 1.248 | | 1.982 |
| O11 | 0.344 | 0.355 | | | 0.078 | 1.208 | | 1.985 |
| O12 | | | | | 0.435 | 1.365 | | 1.800 |
| Σv_{ij} | 1.894 | 1.936 | 2.033 | 2.163 | 2.007 | 5.036 | 5.006 | |

* The values of the bond valence parameters R_o of 1.904 for Cd(II)–O and 1.803 for V(V)–O were used assuming that $b = 0.37$ Å. ** Neglecting H-atom contributions.

Table 5. Hydrogen-bond geometry (Å, °) for Cd₅(VO₄)₂(OH)₄.

| <i>D</i> — <i>H</i> ··· <i>A</i> | <i>D</i> — <i>H</i> | <i>H</i> ··· <i>A</i> | <i>D</i> ··· <i>A</i> | <i>D</i> — <i>H</i> ··· <i>A</i> |
|----------------------------------|---------------------|-----------------------|-----------------------|----------------------------------|
| O1—H1···O12 ⁱⁱⁱ | 0.81(1) | 2.25(3) | 3.017(5) | 157(6) |
| O2—H2···O5 ^{xiii} | 0.82(1) | 2.15(2) | 2.967(5) | 173(6) |
| O3—H3···O12 ^{viii} | 0.82(1) | 2.10(3) | 2.869(5) | 156(6) |
| O4—H4···O7 ^{xiii} | 0.82(1) | 2.10(2) | 2.900(5) | 164(6) |

Symmetry codes: (iii) $-x + 1, y - 1/2, -z + 3/2$; (viii) $x, y, z - 1$; (xiii) $-x + 1/2, -y + 1, z + 1/2$.

3. Results

3.1. Crystal Structure

The asymmetric unit of Cd₅(VO₄)₂(OH)₄ exhibits two crystallographically unique vanadates(V) tetrahedra and five fully occupied Cd sites, each octahedrally coordinated [Cd1O₅(OH), Cd2O₃(OH)₃, Cd3O₄(OH)₂, Cd4O₂(OH)₄, Cd5O₄(OH)₂] (Figure 1). The Cd1 site is coordinated by one OH group and five O atoms, with the <Cd1—OH,O> average distance of 2.351 Å, which is consistent with the bond length statistics and mean Cd—O distance of 2.302 Å [25]. The mean octahedral distances of <2.326>, <2.309>, <2.283>, and <2.359> Å for Cd2O₃(OH)₃, Cd3O₄(OH)₂, Cd4O₂(OH)₄ and Cd5O₄(OH)₂ octahedra, respectively, are also very close to 2.302 Å. They are also close to the value of 2.33 Å (0.95 + 1.38) calculated from the effective ionic radii for divalent cadmium octahedrally coordinated with the six nearest oxygen atoms [26].

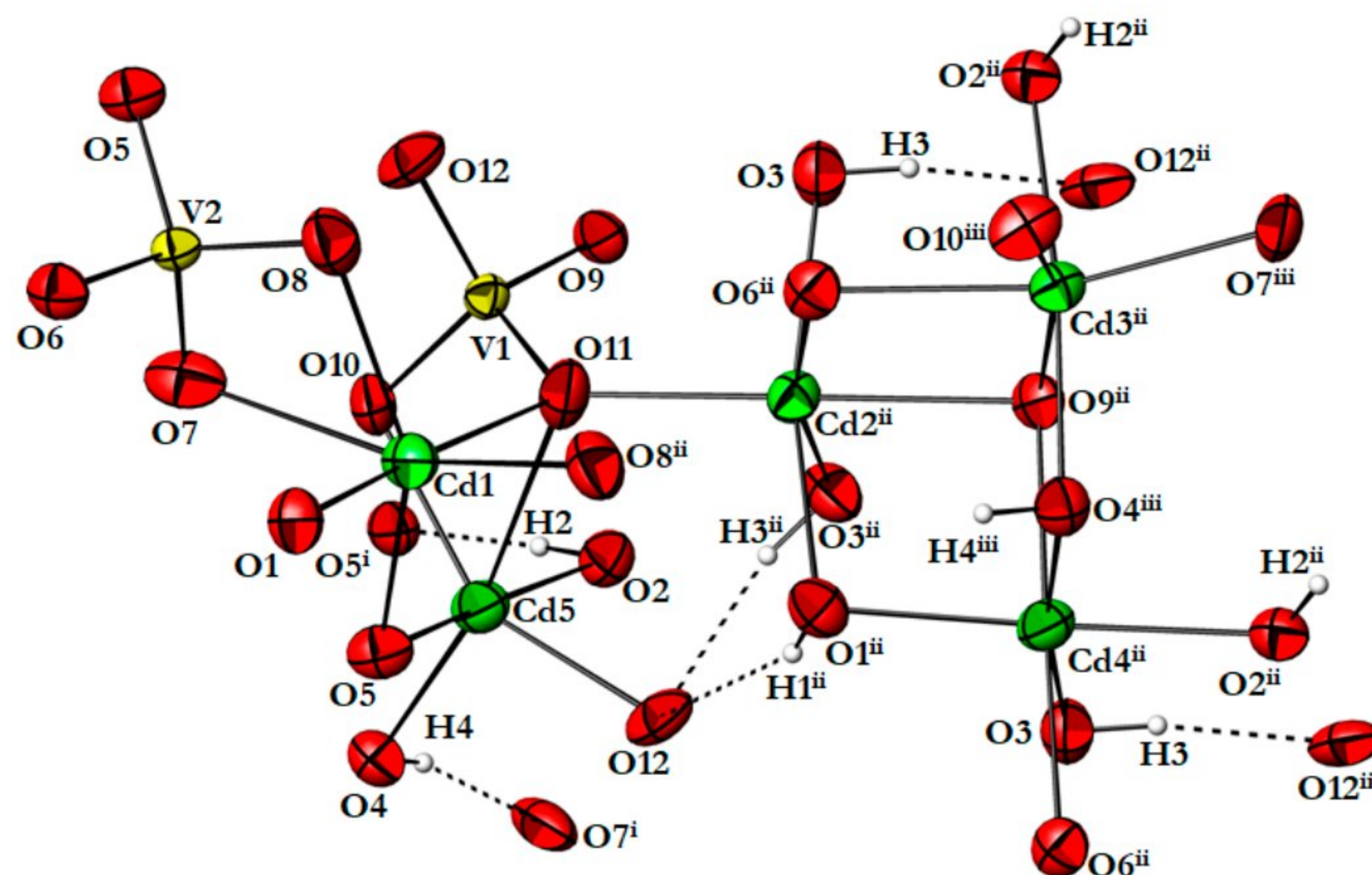


Figure 1. The structural fragment showing ellipsoids of ADP (90% probability), hydrogen bonds, and atomic labeling scheme. Symmetry codes: (i) $-x + 1/2, -y, z + 1/2$; (ii) $-x, y + 1/2, -z + 1/2$; (iii) $x + 1/2, -y + 1/2, -z$.

The bond valence sum calculations [27] for octahedral positions display minor deviations, i.e., all six coordinated Cd atoms have bond valence sums $\sum \nu_{ij}$ close to two (Table 4).

Both V sites are tetrahedrally coordinated with four O atoms. The average <V1,2—O> distances of <1.718> and <1.721> Å, respectively, are in very good agreement with the mean V—O distance of 1.717 Å [25] as well as with the value of 1.735 Å (0.355 + 1.38) calculated from effective ionic radii for tetrahedrally coordinated pentavalent vanadium [26]. The O—V—O angles range from 105.39(19) to 112.87(17)°.

The core of the structure is made of infinite ribbons (Figure 2a), buildup from edge-sharing distorted $M(\text{O},\text{OH})_6$ -octahedra ($M = \text{Cd2}, \text{Cd3}, \text{Cd4}$). Each ribbon, interchangeably

one and two octahedra wide, is extending along [010]. Two adjacent ribbons are further interconnected to infinite double ribbons by sharing O3 vertices, as shown in Figure 2a.

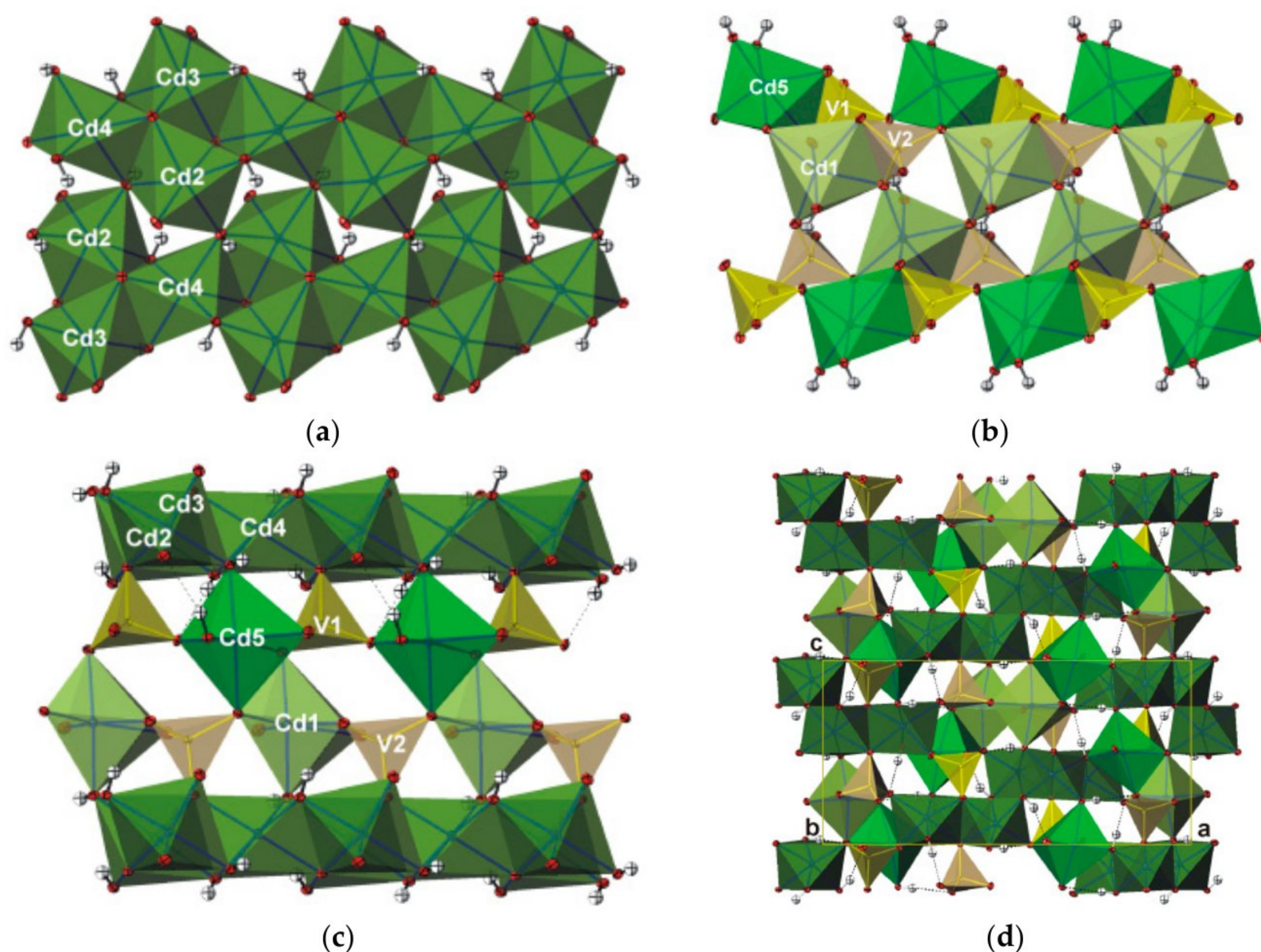


Figure 2. The linkage of two octahedral ribbons of $M(\text{O},\text{OH})_6$ octahedra ($M = \text{Cd}2, \text{Cd}3, \text{Cd}4$) via O3 in the projection approximately along the [101] (b -axis is horizontal). Small grey spheres represent H atoms (a). The linkage of neighboring double chains of coupled VO_4 tetrahedra and $M(\text{O},\text{OH})_6$ octahedra ($M = \text{Cd}1, \text{Cd}5$) via O8 in the projection along the [104] (b -axis is horizontal) (b). The double ribbons of $M(\text{O},\text{OH})_6$ octahedra ($M = \text{Cd}2, \text{Cd}3, \text{Cd}4$) connected by pairs of coupled VO_4 tetrahedra and $M(\text{O},\text{OH})_6$ octahedra ($M = \text{Cd}1, \text{Cd}5$) (c). The projection of the structure along the [010] direction (d).

The $\text{V}1\text{O}_4$ tetrahedra and $\text{Cd}5\text{O}_4(\text{OH})_2$ octahedra share a common edge as well as the $\text{V}2\text{O}_4$ tetrahedra and $\text{Cd}1\text{O}_5(\text{OH})$ octahedra. Thus, they form two polyhedral pairs. Each pair $\text{VO}_4\text{-CdO}_5(\text{OH})$ of coupled polyhedra is bonded to adjacent similar pairs sharing common vertices and forming $[\text{V}1\text{O}_4\text{-Cd}5\text{O}_4(\text{OH})_2]_n$ and $[\text{V}2\text{O}_4\text{-Cd}1\text{O}_5(\text{OH})]_n$ chains in the [010] direction (Figure 2b). These two adjacent chains are further interconnected by edge-shared $M(\text{O},\text{OH})_6$ ($M = \text{Cd}1, \text{Cd}5$) octahedra forming double chains of coupled polyhedra $[\text{V}1\text{O}_4\text{-Cd}5\text{O}_4(\text{OH})_2\text{-Cd}1\text{O}_5(\text{OH})\text{-V}2\text{O}_4]_n$ and running along the same [010] direction.

Two neighboring double chains are additionally connected via O8 vertices (Figure 2b). The double ribbons of $M(\text{O},\text{OH})_6$ octahedra ($M = \text{Cd}2, \text{Cd}3, \text{Cd}4$) are connected by pairs of coupled VO_4 tetrahedra and $M(\text{O},\text{OH})_6$ octahedra ($M = \text{Cd}1, \text{Cd}5$) sharing vertices (Figure 2c). The $\text{O-H}\cdots\text{O}$ hydrogen bonds additionally link the two subunits, the ribbons, and chains into a three-dimensional structure (Figure 2d).

The V cations in double chains are separated from each other by 4.1214(9) Å, which is slightly less than the sum of the van der Waals radii [28,29] of 4.26 Å [2×2.13]. Several V–Cd distances are also less than the sum of the van der Waals radii of 3.71 Å [$r_{\text{Cd}} + r_{\text{V}} = 1.58 + 2.13$]. The distances between the V1 and Cd neighbors are ranging from 3.0934(7) to 3.5678(8) Å, which is similar to the distances of V2 and Cd neighbors that are in the range from 3.1081(7) to 3.4731(7) Å. The shortest V1–Cd5 and V2–Cd1 contacts are found in coupled polyhedra where they are 3.0934(7) and 3.1081(7) Å, respectively. All Cd–Cd distances are longer than the sum of the van der Waals radii of 3.16 Å [2×1.58] [28], and they are in the interval from 3.4575(7) to 3.5961(8) Å.

Hydrogen bonding (Table 5) plays a significant role in linking the double ribbons with the double chains of coupled polyhedra. This interaction contributes to the stability of the structure. Bond valence analysis shows that considering the contribution of non-hydrogen atoms only, the O1, O2, O3, and O4 atoms are all undersaturated (Σv_{ij} are 1.125, 1.079, 1.116, and 1.237 v.u.) as well as O5, O7, and O12 (Σv_{ij} are 1.834, 1.805 and 1.800 v.u.). Considering that the O1, O2, O3, and O4 atoms are hydrogen bond donors, O5 and O7 are single acceptors and O12 is a double acceptor of middle strong and weak hydrogen bonds; the bond valences are well balanced. The total amount of the bond strengths, including the contribution of the hydrogen bonds, are in excellent agreement with the expectations.

3.2. Raman Spectrometry

The Raman spectrum is shown in Figure 3. It reflects the complexity of the crystal structure. Bands in the high-energy range (3100–3600 cm^{-1}) are due to the stretching of O–H bonds of hydroxyl groups. Bands in the 100–1100 cm^{-1} range are caused by internal vibrations either of VO_4 tetrahedra or due to external vibrational modes.

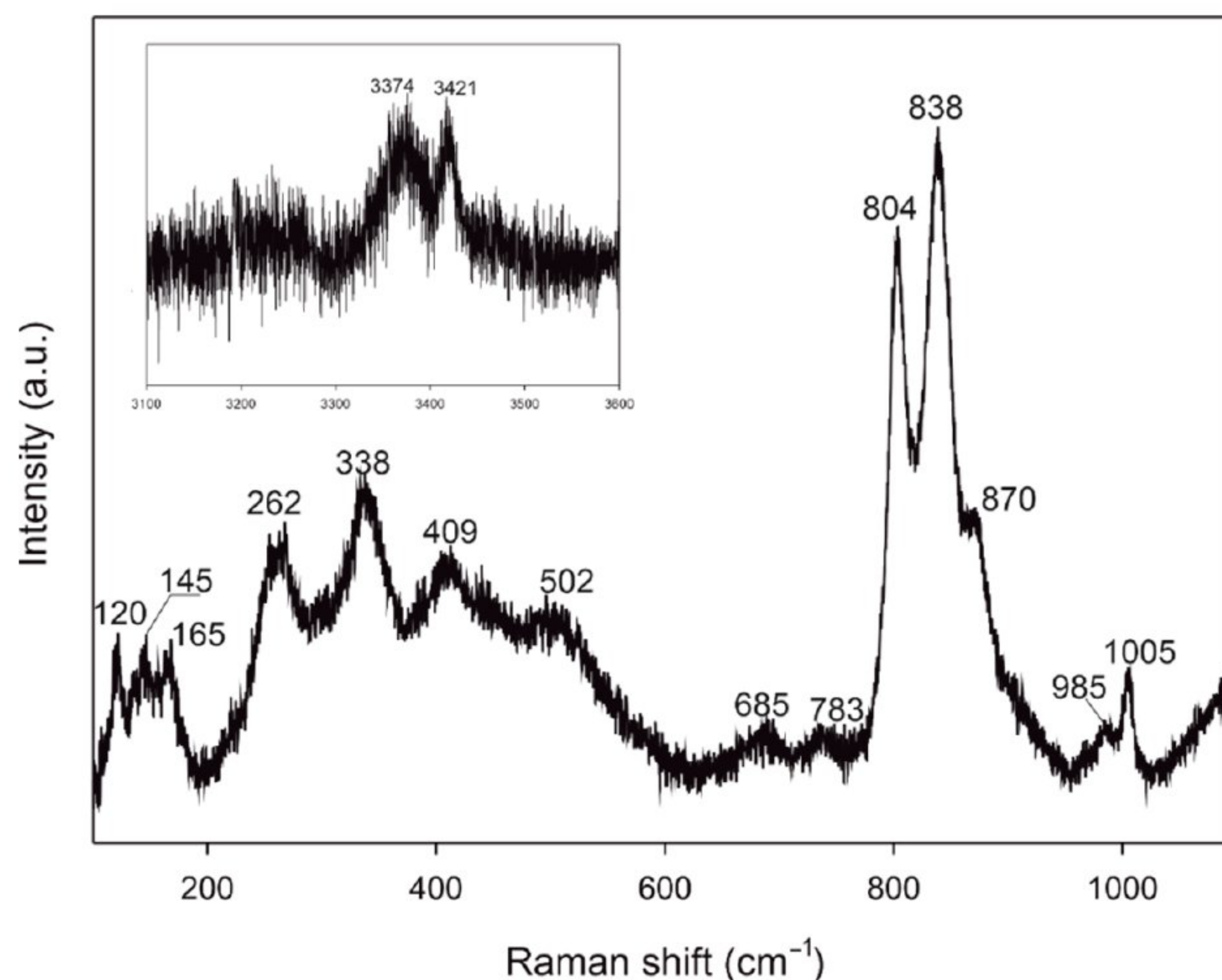


Figure 3. The Raman spectrum of $\text{Cd}_5(\text{VO}_4)_2(\text{OH})_4$ between 100 and 1100 cm^{-1} and the section between 3100 and 3600 cm^{-1} showing the OH stretching region.

According to the d – ν correlation for hydrogen bonds [30], the Raman-shift values observed in the O–H stretching region (Figure 3) are in very good agreement with the refined O–H \cdots O bond lengths between 2.869(5) and 3.017(5) Å (Raman bands obtained at 3374 and 3421 cm^{-1}).

In the 600–900 cm^{-1} spectral range, the Raman bands could be assigned to symmetric and antisymmetric stretching modes of the $(\text{VO}_4)^{3-}$ groups whereas internal bending vibrations of these tetrahedra are observed below 550 cm^{-1} , here, partially overlaid by various external modes (Figure 3). Precisely, the Raman spectrum of $\text{Cd}_5(\text{VO}_4)_2(\text{OH})_4$ is characterized by three intense bands at 870 (m), 838 (vs), and 804 (s) cm^{-1} assigned to ν_1 $(\text{VO}_4)^{3-}$ symmetric stretching modes and two weak bands around 685 and 783 cm^{-1} assigned to the ν_3 $(\text{VO}_4)^{3-}$ antisymmetric stretching modes. The symmetric stretches of $\text{Cd}_5(\text{VO}_4)_2(\text{OH})_4$ compare well with the symmetric stretches of the synthetic $\text{SrCu}(\text{OH})(\text{VO}_4)$ [15], which has stretching modes that lie around 883 (w), 840 (vs), 810 (s), 786 (w), and 750 (w) cm^{-1} .

4. Discussion and Relationships to Similar Structures

The synthetic compound $\text{Cd}_5(\text{VO}_4)_2(\text{OH})_4$ is isostructural with the minerals arsenoclasite, $\text{Mn}(\text{II})_5(\text{AsO}_4)_2(\text{OH})_4$ [31], and its phosphate analog gatehouseite, $\text{Mn}(\text{II})_5(\text{PO}_4)_2(\text{OH})_4$ [23]. Pring and Birch [32] refined the structure of gatehouseite in the same space group $P2_12_12_1$ but in a $c\bar{b}a$ setting. It is also isostructural with two synthetic compounds, $\text{Mn}_5(\text{PO}_4)_2(\text{OH})_4$ and $\text{Co}_5(\text{PO}_4)_2(\text{OH})_4$, [33] refined with cyclically permuted abc axes in a cab setting (Table 6). This small family of compounds belongs to a $\text{Co}_5(\text{PO}_4)_2(\text{OH})_4$ structure type, exhibits the same symmetry and topology (Figure 4a,b), and has the general formula $M_5(\text{XO}_4)_2(\text{OH})_4$ where M is a divalent Cd, Mn, or Co cation, and X is a pentavalent P, As, or V cation. Topologically, the edge-shared Cd triangle patterns can be described as the corrugated layer parallel to (001) and approximately half c -axis wide (Figure 4b). Each layer consists of ribbons, which are parallel to [010] and connected by an array of Cd1 atoms (Figure 4a).

In spite of their identical stoichiometry, other $M_5(\text{XO}_4)_2(\text{OH})_4$ compounds have lower symmetry and adopt different structure types (Table 6). One structural group that includes mineral reppiaite, $\text{Mn}_5(\text{PO}_4)_2(\text{OH})_4$ [2,34], isostructural synthetic compound $\text{Ni}_5(\text{AsO}_4)_2(\text{OH})_4$ [35] as well as minerals cornubite, $\text{Cu}_5(\text{AsO}_4)_2(\text{OH})_4$ [36–38] and turanite, $\text{Cu}_5(\text{VO}_4)_2(\text{OH})_4$, [3,39] corresponds to the layer structures. These are built from alternating octahedral and tetrahedral more or less distorted, basically flat layers which form a 3D framework. While octahedral layers of reppiaite and turanite have the same topology, those of cornubite have different topologies resulting from different patterns of octahedral distortions and vacancy distributions (Figure 4c–e).

The patterns of Mn triangles in reppiaite and Cu triangles in turanite can be described as consisting of two types of chains parallel to [001] in reppiaite and to [100] in turanite. One chain is a buildup of alternating edge- and corner-sharing triangles and one with centered hexagons. In cornubite, one type of chain contains only edge-sharing Cu triangles parallel to the a -axis, and the other contains empty hexagons.

The chemical features of $\text{Cd}_5(\text{VO}_4)_2(\text{OH})_4$ are also related to the three polymorphs of $\text{Cu}_5(\text{PO}_4)_2(\text{OH})_4$ minerals [40–42]: pseudomalachite [43], reichenbachite [44–46], ludjibaite [40,47], and the As analog of pseudomalachite, mineral cornwallite, $\text{Cu}_5(\text{AsO}_4)_2(\text{OH})_4$ [48]. The structures of these three polymorphs are also characterized by layers of edge-sharing copper coordination octahedra joined in the third dimension by phosphate (arsenate) tetrahedra. Topologically, they are similar mutually but quite different from the other $M_5(\text{XO}_4)_2(\text{OH})_4$ compounds (Figure 4h). In pseudomalachite and ludjibaite, which are topologically identical, two different types of chains parallel to [010] are also found. In both structures, chains of type I are formed by triangles sharing edges and vertices, and the chains of type II are created by sharing vertices only. In this way, the Cu patterns contain three- and five-membered rings. The pattern in pseudomalachite is a distorted version of the pattern in ludjibaite. The very distorted Cu lattice of reichenbachite is also formed from three- and five-membered rings that share common edges and vertices, but it is principally different from those in pseudomalachite and ludjibaite.

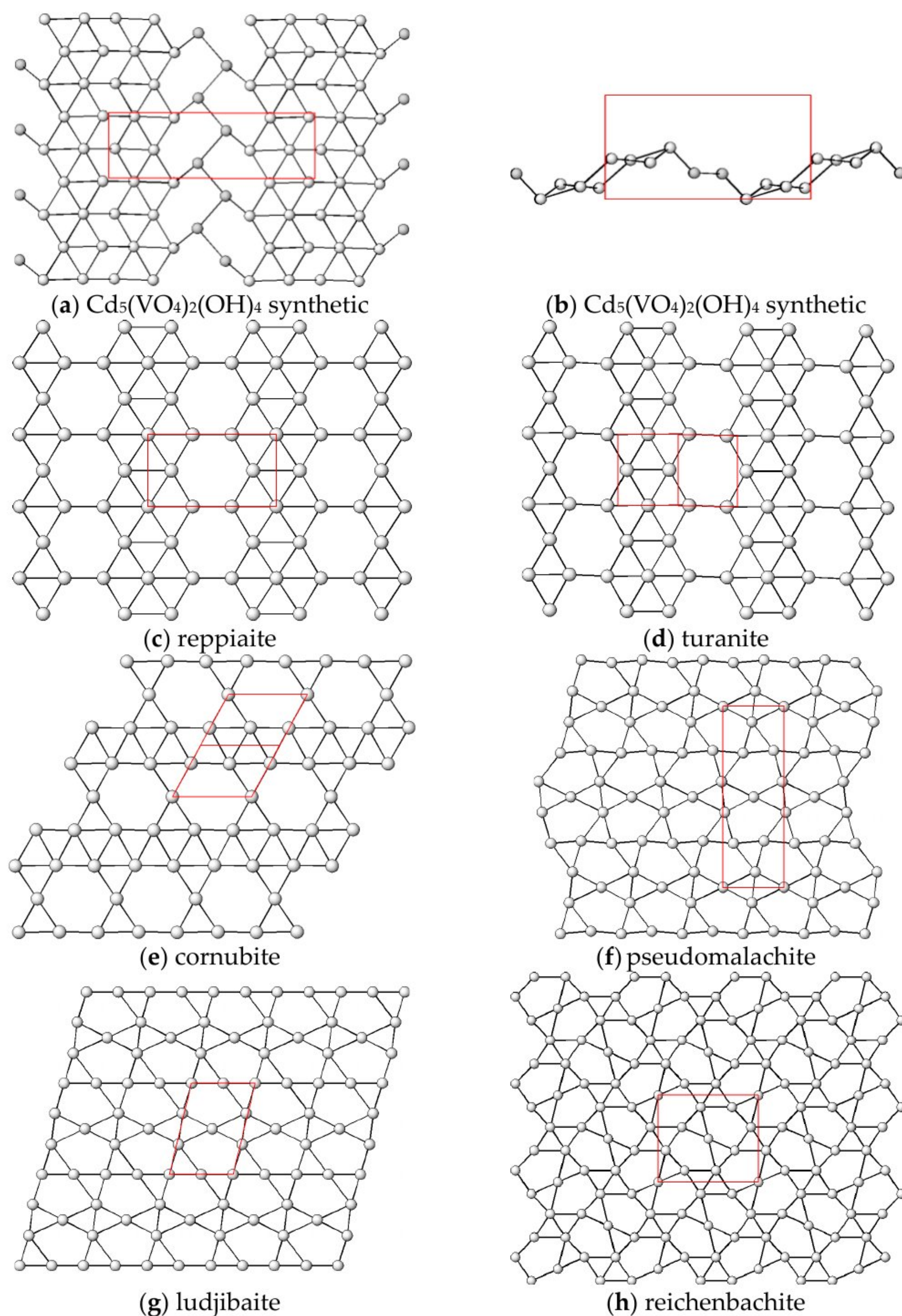


Figure 4. The nodal representation (nodes symbolize MO_6 octahedra) of different topologies observed in $\text{M}_5(\text{XO}_4)_2(\text{OH})_4$ compounds. The solid lines represent $\text{M}\cdots\text{M}$ interatomic distances shorter than 4 \AA . A trace of the unit cell is drawn for reference (red). The projection (a) along the c -axis direction in synthetic $\text{Cd}_5(\text{VO}_4)_2(\text{OH})_4$ (Cd1O_6 octahedra are grey); (b) along the b -axis direction in synthetic $\text{Cd}_5(\text{VO}_4)_2(\text{OH})_4$ (The similar metal wavy layers were found in arsenoclasite, $\text{Mn}_5(\text{AsO}_4)_2(\text{OH})_4$, gatehouseite, $\text{Mn}_5(\text{PO}_4)_2(\text{OH})_4$, as well as in synthetic $\text{Co}_5(\text{PO}_4)_2(\text{OH})_4$); (c) along a -axis in reppiaite, $\text{Mn}_5(\text{OH})_4(\text{VO}_4)_2$; (d) along $[0 \bar{1} \bar{1}]$ in turanite, $\text{Cu}_5(\text{OH})_4(\text{VO}_4)_2$; (e) along $[01 \bar{1}]$ in cornubite, $\text{Cu}_5(\text{AsO}_4)_2(\text{OH})_4$; (f) along a -axis in pseudomalachite, $\text{Cu}_5(\text{PO}_4)_2(\text{OH})_4$ and cornwallite, $\text{Cu}_5(\text{AsO}_4)_2(\text{OH})_4$; (g) along a -axis in ludjibaite, $\text{Cu}_5(\text{PO}_4)_2(\text{OH})_4$; (h) along c -axis in reichenbachite, $\text{Cu}_5(\text{PO}_4)_2(\text{OH})_4$.

Table 6. Comparison of the unit cell parameters of analogous structures of $M_5(XO_4)_2(OH)_4$ compounds.

| Compound Mineral Name | $a(\text{Å}), b(\text{Å}), c(\text{Å})$ | $\alpha(^{\circ}), \beta(^{\circ}), \gamma(^{\circ})$ | $V(\text{Å}^3)$ | Space Group | Reference |
|---|---|---|-----------------|--------------|-----------|
| $Mn_5(AsO_4)_2(OH)_4$ arsenoclasite | 18.290(20) 5.75(1) 9.31(2) | 90, 90, 90 | 979.11 | $P2_12_12_1$ | [31] |
| $Mn_5(P_{0.88}Si_{0.09}As_{0.03}O_4)_2(OH)_4$ gatehouseite | 17.9733(18) 5.6916(11) 9.130(4) | 90, 90, 90 | 933.9 (3) | $P2_12_12_1$ | [23] |
| $Mn_{5.09}Fe_{0.01}Al_{0.01}(OH)_4$ $(P_{0.90}As_{0.09}V_{0.01}O_4)_2(OH)_4$ gatehouseite | 9.097(2) 5.693(2) 18.002(10) | 90, 90, 90 | 932.4 (8) | $P2_12_12_1$ | [32] |
| $Mn_5(PO_4)_2(OH)_4$ gatehouseite synthetic | 9.110(1) 18.032(4) 5.6923(6) | 90, 90, 90 | 935.08 | $P2_12_12_1$ | [33] |
| $Co_5(PO_4)_2(OH)_4$ gatehouseite type synthetic | 8.903(2) 17.397(2) 5.5154(4) | 90, 90, 90 | 854.26 | $P2_12_12_1$ | [33] |
| $Cd_5(VO_4)_2(OH)_4$ gatehouseite type synthetic | 19.011(4) 6.0133(12) 9.5411(19) | 90, 90, 90 | 1090.7 (4) | $P2_12_12_1$ | This work |
| $Mn_5(V_{0.89}As_{0.11}O_4)_2(OH)_4$ reppiaite | 9.604(2) 9.558(2) 5.393(1) | 90, 98.45(1), 90 | 489.68 | $C2/m$ | [34] |
| $Ni_5(AsO_4)_2(OH)_4$ reppiaite type synthetic | 9.291(2) 9.008(2) 5.149(1) | 90, 98.70(3), 90 | 425.98 | $C2/m$ | [35] |
| $Cu_5(VO_4)_2(OH)_4$ turanite | 5.3834(2) 6.2736(3) 6.8454(3) | 86.169(1), 91.681(1),92.425(1) | 230.38 (2) | $P\bar{1}$ | [39] |
| $Cu_5(AsO_4)_2(OH)_4$ cornubite | 6.121(1) 6.251(1) 6.790(1) | 92.93(1), 111.30(1),107.47(1) | 227.11 | $P\bar{1}$ | [36] |
| $Cu_5(PO_4)_2(OH)_4$ pseudomalachite | 4.4728(4) 5.7469(5) 17.032(3) | 90, 91.043(7), 90 | 437.73 | $P2_1/c$ | [43] |
| $Cu_5(AsO_4)_2(OH)_4$ cornwallite | 4.600(2) 5.757(3) 17.380(6) | 90, 91.87 (3), 90 | 460.02 | $P2_1/c$ | [48] |
| $Cu_5(PO_4)_2(OH)_4$ reichenbachite synthetic | 9.186(2) 10.684(2) 4.461(1) | 90, 92.31(1), 90 | 437.46 | $P2_1/a$ | [44] |
| $Cu_5(PO_4)_2(OH)_4$ ludjibaite | 4.445(1) 5.873(1) 8.668(3) | 103.62(2), 90.35(2), 93.02(1) | 219.57 | $P\bar{1}$ | [49] |

5. Conclusions

The hydrothermally obtained title compound $Cd_5(VO_4)_2(OH)_4$ is the second known compound next to $Cd(VO_3)_2 \cdot 4H_2O$ [16] synthesized in the $CdO-V_2O_5-H_2O$ system. It belongs to a small family of compounds adopting the $Co_5(PO_4)_2(OH)_4$ structure type. These compounds exhibit $P2_12_12_1$ symmetry and have the general formula $M_5(XO_4)_2(OH)_4$, where M is a divalent Cd, Mn, or Co cation, and X is a pentavalent P, As, or V cation. Other $M_5(XO_4)_2(OH)_4$ compounds have lower symmetry, different structure types, and topologies.

Numerous metal vanadates have been widely studied during the last decades due to their promising properties. Special interest in transition metal vanadates is due to their interesting optical, electric, and magnetic properties and thus can be used in (photo)catalysis, lithium-ion batteries, solar cells, gas sensors, water-splitting technologies, and optoelectronics [50] and references therein.

Detailed study of the selected metal–vanadate systems would lead to a detailed understanding of which topologies and affinities are likely to form under which conditions (e.g., pH, ratios of ionic radii, temperature, etc.). This information could also be useful not only to vanadates but also to phosphates, arsenates, and maybe silicates, whose technological usage is built on the special physical and chemical performance that is basically dependent on their crystal structure.

Author Contributions: Conceptualization, L.K. and T.Đ.; methodology, T.Đ.; formal analysis, L.K. and T.Đ.; investigation, L.K. and T.Đ.; resources, T.Đ.; data curation, L.K. and T.Đ.; writing—original draft preparation L.K.; writing—review and editing, L.K. and T.Đ.; visualization, L.K. and T.Đ.; project administration, T.Đ.; funding acquisition, T.Đ. All authors have read and agreed to the published version of the manuscript.

Funding: This research was funded by the Austrian Science Foundation (FWF) (grant No. V203-N19) and is gratefully acknowledged.

Data Availability Statement: The supplementary crystallographic data for this paper (deposition number 2221388) are provided free of charge by the joint Cambridge Crystallographic Data Centre and Fachinformationszentrum Karlsruhe Access Structures service www.ccdc.cam.ac.uk/structures (accessed on 21 November 2022).

Acknowledgments: Two anonymous reviewers are thanked for their careful corrections and comments, which helped to improve the manuscript.

Conflicts of Interest: The authors declare no conflict of interest.

References

1. Puzio, B.; Manecki, M. The prediction method for standard enthalpies of apatites using the molar volume, lattice energy, and linear correlations from existing experimental data. *Contrib. Mineral. Petrol.* **2022**, *177*, 103–137. [[CrossRef](#)]
2. Yakubovich, O.; Kiriukhina, G. A mero-plesiotype series of vanadates, arsenates and phosphates with blocks based on densely packed octahedral layers as repeating modules. *Minerals* **2021**, *11*, 273. [[CrossRef](#)]
3. Zhang, S.Y.; Guo, W.B.; Yang, M.; Tang, Y.Y.; Cui, M.Y.; Wang, N.N.; He, Z.Z. A frustrated ferrimagnet $\text{Cu}_5(\text{VO}_4)_2(\text{OH})_4$ with a 1/5 magnetization plateau on a new spin-lattice of alternating triangular and honeycomb strips. *Dalton Trans.* **2015**, *44*, 20562–20567. [[CrossRef](#)]
4. Machida, M.; Miyazaki, Y.; Matsunaga, Y.; Ikeue, K. Efficient catalytic decomposition of sulfuric acid with copper vanadates as an oxygen-generating reaction for solar thermochemical water splitting cycles. *Chem. Commun.* **2011**, *47*, 9591–9593. [[CrossRef](#)] [[PubMed](#)]
5. Li, D.; Bai, X.; Pan, C.; Zhu, Y. Investigations on the Phase Transition between CdV_2O_6 and $\text{Cd}_2\text{V}_2\text{O}_7$ and their photocatalytic performances. *Eur. J. Inorg. Chem.* **2013**, *2013*, 3070–3075. [[CrossRef](#)]
6. Oshikiri, M.; Boero, M.; Ye, J.; Zou, Z.; Kido, G. Electronic structures of promising photocatalysts InMO_4 , $M = \text{V, Nb, Ta}$... and BiVO_4 for water decomposition in the visible wavelength region. *J. Chem. Phys.* **2002**, *117*, 7313–7318. [[CrossRef](#)]
7. Wang, D.; Tang, J.; Zou, Z.; Ye, J. Photophysical and photocatalytic properties of a new series of visible-light-driven photocatalysts $M_3\text{V}_2\text{O}_8$ ($M = \text{Mg, Ni, Zn}$). *Chem. Mater.* **2005**, *17*, 5177–5182. [[CrossRef](#)]
8. Shi, R.; Wang, Y.; Zhou, F.; Zhu, Y. $\text{Zn}_3\text{V}_2\text{O}_7(\text{OH})_2(\text{H}_2\text{O})_2$ and $\text{Zn}_3\text{V}_2\text{O}_8$ nanostructures: Controlled fabrication and photocatalytic performance. *J. Mater. Chem.* **2011**, *21*, 6313–6320. [[CrossRef](#)]
9. Huang, Y.; Yu, Y.M.; Tsuboi, T.; Seo, H.J. Novel yellow-emitting phosphors of $\text{Ca}_5\text{M}_4(\text{VO}_4)_6$ ($M = \text{Mg, Zn}$) with isolated VO_4 tetrahedra. *Opt. Express* **2012**, *20*, 4360–4368. [[CrossRef](#)]
10. Djemal, A.; Louati, B.; Guidara, K. Synthesis and characterization of orthovanadates compounds $\text{Li}_{(1-x)}\text{Na}_x\text{CdVO}_4$ ($x = 0, 0.25$). *J. Alloys Compd.* **2016**, *683*, 610–618. [[CrossRef](#)]
11. Đorđević, T.; Karanović, L.; Tillmanns, E. Structural and spectroscopic study of $\text{Mg}_{13.4}(\text{OH})_6(\text{HVO}_4)_2(\text{H}_0.2\text{VO}_4)_6$. *Cryst. Res. Technol.* **2008**, *43*, 1202–1209. [[CrossRef](#)]
12. Đorđević, T.; Stojanović, J.; Karanović, L. $\text{Zn}_{1.86}\text{Cd}_{0.14}(\text{OH})\text{VO}_4$. *Acta Cryst.* **2010**, *E66*, i79. [[CrossRef](#)] [[PubMed](#)]
13. Đorđević, T.; Karanović, L. $\text{Ba}[\text{Co}_3(\text{VO}_4)_2(\text{OH})_2]$ with a regular Kagome lattice. *Acta Cryst.* **2013**, *C69*, 114–118. [[CrossRef](#)] [[PubMed](#)]

14. Đorđević, T.; Karanović, L. A new anion-deficient fluorite-related superstructure of $\text{Bi}_{28}\text{V}_8\text{O}_{62}$. *J. Solid State Chem.* **2014**, *220*, 259–269. [[CrossRef](#)]
15. Đorđević, T.; Kolitsch, U.; Nasdala, L. A single-crystal X-ray and Raman spectroscopic study of hydrothermally synthesized arsenates and vanadates with the descloizite and adelite structure types. *Am. Mineral.* **2016**, *101*, 1135–1149. [[CrossRef](#)]
16. Ulická, L. Crystal structure of $\text{Cd}(\text{VO}_3)_2 \cdot 4\text{H}_2\text{O}$ and its comparison with the structure of $\text{Ca}(\text{VO}_3)_2 \cdot 4\text{H}_2\text{O}$ and $\alpha\text{-Cd}(\text{VO}_3)$. *Chem. Pap.* **1988**, *42*, 11–19.
17. Nonius. *COLLECT Data Collection Software, 2005–2007*; Nonius BV: Delft, The Netherlands, 2002.
18. Otwinowski, Z.; Minor, W. Processing of X-ray Diffraction Data Collected in Oscillation Mode. In *Methods in Enzymology*; Carter, J.C.W., Sweet, R.M., Eds.; Academic Press: New York, NY, USA, 1997; Volume 276, pp. 307–326.
19. Otwinowski, Z.; Borek, D.; Majewski, W.; Minor, W. Multiparametric scaling of diffraction intensities. *Acta Cryst.* **2003**, *A59*, 228–234. [[CrossRef](#)]
20. Sheldrick, G.M. SHELXT—Integrated space-group and crystal structure determination. *Acta Cryst.* **2015**, *A71*, 3–8. [[CrossRef](#)]
21. Sheldrick, G.M. Crystal structure refinement with SHELXL. *Acta Cryst.* **2015**, *C71*, 3–8.
22. Farrugia, L.J. WinGX and ORTEP for Windows: An update. *J. Appl. Cryst.* **2012**, *45*, 849–854. [[CrossRef](#)]
23. Elliott, P.; Pring, A. The crystal structure of gatehouseite. *Mineral. Mag.* **2011**, *75*, 2823–2832. [[CrossRef](#)]
24. Dowty, E. *ATOMS for Windows*; Version 5.1; Shape Software: Kingsport, TN, USA, 2000.
25. Gagné, O.C.; Hawthorne, F.C. Bond-length distributions for ions bonded to oxygen: Results for the transition metals and quantification of the factors underlying bond-length variation in inorganic solids. *IUCrJ* **2020**, *7*, 581–629. [[CrossRef](#)] [[PubMed](#)]
26. Shannon, R.D. Revised effective ionic radii and systematic studies of interatomic distances in halides and chalcogenides. *Acta Cryst.* **1976**, *A32*, 751–767. [[CrossRef](#)]
27. Brown, I.D.; Altermatt, D. Bond-Valence Parameters Obtained from a Systematic Analysis of the Inorganic Crystal Structure Database. *Acta Cryst.* **1985**, *B41*, 244–247. [[CrossRef](#)]
28. Bondi, A. Van der Waals Volumes and Radii. *J. Phys. Chem.* **1964**, *68*, 441–451. [[CrossRef](#)]
29. Spek, A.L. Single-crystal structure validation with the program PLATON. *J. Appl. Cryst.* **2003**, *36*, 7–13. [[CrossRef](#)]
30. Libowitzky, E. Correlation of O–H stretching frequencies and O–H···O hydrogen bond lengths in minerals. *Mon. Chem.* **1999**, *130*, 1047–1059. [[CrossRef](#)]
31. Moore, P.B.; Molin-Case, J. Crystal chemistry of the basic manganese arsenates: V. Mixed manganese coordination in the atomic arrangement of arsenoclasite. *Am. Mineral.* **1971**, *56*, 1539–1552.
32. Pring, A.; Birch, W.D. Gatehouseite, a new manganese hydroxy phosphate from Iron Monarch, South Australia. *Mineral. Mag.* **1993**, *57*, 309–313. [[CrossRef](#)]
33. Ruzsala, F.A.; Anderson, J.B.; Kostiner, E. Crystal structures of two isomorphs of arsenoclasite: $\text{Co}_5(\text{PO}_4)_2(\text{OH})_4$ and $\text{Mn}_5(\text{PO}_4)_2(\text{OH})_4$. *Inorg. Chem.* **1977**, *16*, 2417–2422. [[CrossRef](#)]
34. Basso, R.; Lucchetti, G.; Zefiro, L.; Palenzona, A. Reppiaite, $\text{Mn}_5(\text{OH})_4(\text{VO}_4)_2$, a new mineral from Val Graveglia (Northern Apennines, Italy). *Z. Kristallogr.* **1992**, *201*, 223–234. [[CrossRef](#)]
35. Barbier, J. Crystal structure of $\text{Ni}_5(\text{AsO}_4)_2(\text{OH})_4$ and its comparison to other $\text{M}_5(\text{XO}_4)_2(\text{OH})_4$ compounds. *Eur. J. Mineral.* **1996**, *8*, 77–84. [[CrossRef](#)]
36. Sieber, N.H.W.; Hofmeister, W.; Tillmanns, E.; Abraham, K. Neue mineraldaten für kupferphosphate und-arsenate von Reichenbach/Odw. *Fortschr. Mineral.* **1984**, *62*, 231–232.
37. Tillmanns, E.; Hofmeister, W.; Petitjean, K. Cornubite, $\text{Cu}_5(\text{AsO}_4)_2(\text{OH})_4$, first occurrence of single crystals, mineralogical description and crystal structure. *Bull. Geol. Soc. Finland* **1985**, *57*, 119–127. [[CrossRef](#)]
38. Janeczek, J.; Ciesielczuk, J.; Dulski, M.; Krzykowski, T. Chemical composition and Raman spectroscopy of cornubite and its relation to cornwallite in Miedzianka, the Sudety Mts, Poland. *N. Jb. Miner. Abh.* **2016**, *193*, 265–274. [[CrossRef](#)]
39. Sokolova, E.V.; Hawthorne, F.C.; Karpenko, V.Y.; Agakhanov, A.A.; Pautov, L.A. Turanite, $\text{Cu}_5(\text{VO}_4)_2(\text{OH})_4$, from the Tyuya-Muyun radium-uranium deposit, Osh Region, Kyrgyzstan: A new structure for an old mineral Locality: Osh Region, Kyrgyzstan. *Can. Mineral.* **2004**, *42*, 731–739. [[CrossRef](#)]
40. Martens, W.N.; Frost, R.L.; Williams, P.A. The basic copper phosphate minerals pseudomalachite, ludjibaite and reichenbachite: An infrared emission and Raman spectroscopic study. *N. Jb. Miner. Mh.* **2003**, *2003*, 337–362. [[CrossRef](#)]
41. Krivovichev, S.V.; Zolotarev, A.A.; Popova, V.I. Hydrogen bonding and structural complexity in the $\text{Cu}_5(\text{PO}_4)_2(\text{OH})_4$ polymorphs (pseudomalachite, ludjibaite, reichenbachite): Combined experimental and theoretical study. *Struct. Chem.* **2016**, *27*, 1716–1723. [[CrossRef](#)]
42. Makovicky, E. The pseudomalachite-ludjibaite-reichenbachite conundrum: OD description. *Can. Mineral.* **2019**, *57*, 571–581. [[CrossRef](#)]
43. Shoemaker, G.L.; Anderson, J.B.; Kostiner, E. Refinement of the crystal structure of pseudomalachite. *Am. Mineral.* **1977**, *62*, 1042–1048.
44. Anderson, J.B.; Shoemaker, G.L.; Kostiner, E.; Ruzsala, F.A. The crystal structure of synthetic $\text{Cu}_5(\text{PO}_4)_2(\text{OH})_4$, a polymorph of pseudomalachite. *Am. Mineral.* **1977**, *62*, 115–121.
45. Sieber, N.H.W.; Tillmanns, E.; Medenbach, O. Hentschelite, $\text{CuFe}_2(\text{PO}_4)_2(\text{OH})_2$, a new member of the lazulite group, and reichenbachite, $\text{Cu}_5(\text{PO}_4)_2(\text{OH})_4$, a polymorph of pseudomalachite, two new copper phosphate minerals from Reichenbach, Germany. *Am. Mineral.* **1987**, *72*, 404–408.

46. Braithwaite, R.S.W.; Ryback, G. Reichenbachite from Cornwall and Portugal. *Mineral. Mag.* **1994**, *58*, 449–451. [[CrossRef](#)]
47. Piret, P.; Deliens, M. Description de la ludjibaïte, un polymorphe de la pseudomalachite, $\text{Cu}_5(\text{PO}_4)_2(\text{OH})_4$. *Bull. Mineral.* **1988**, *111*, 167–171. [[CrossRef](#)]
48. Arlt, T.; Armbruster, T. Single-crystal X-ray structure refinement of cornwallite, $\text{Cu}_5(\text{AsO}_4)_2(\text{OH})_4$: A comparison with its polymorph cornubite and the (PO_4) -analogue pseudomalachite. *Neues Jahrb. Mineral. Monatsh.* **1999**, *10*, 468–480.
49. Shoemaker, G.L.; Anderson, J.B.; Kostiner, E. The crystal structure of a third polymorph of $\text{Cu}_5(\text{PO}_4)_2(\text{OH})_4$. *Am. Mineral.* **1981**, *66*, 169–181.
50. Monfort, O.; Petrisková, P. Binary and ternary vanadium oxides: General overview, physical properties, and photochemical processes for environmental applications. *Processes* **2021**, *9*, 214. [[CrossRef](#)]